Int J Appl Earth Obs Geoinformation 79 (2019) 153–161

Contents lists available at ScienceDirect

Int J Appl Earth Obs Geoinformation

journal homepage: www.elsevier.com/locate/jag

Estimation of suspended sediment concentration in an intermittent river using multi-temporal high-resolution satellite imagery

Francisco Jairo Soares Pereira[a], Carlos Alexandre Gomes Costa[a], Saskia Foerster[b], Arlena Brosinsky[b,c], José Carlos de Araújo[a,*]

[a] Department of Agricultural Engineering, Federal University of Ceará, Fortaleza, Brazil
[b] GFZ German Research Centre for Geosciences, Section 1.4 Remote Sensing, Telegrafenberg, 14473 Potsdam, Germany
[c] University of Potsdam, Institute of Earth and Environmental Science, Karl-Liebknecht-Str. 24–25, 14476 Potsdam-Golm, Germany

ARTICLE INFO

Keywords:
Remote sensing
Sediment load
Dryland
Brazil

ABSTRACT

There is a shortage of sediment-routing monitoring worldwide, despite its relevance to environmental processes. In drylands, where water resources are more vulnerable to the sediment dynamics, this flaw is even more harmful. In the semi-arid Caatinga biome in the North-east of Brazil, rivers are almost all intermittent and hydro-sedimentological monitoring is scarce. In the biome, water supply derives from thousands of surface reservoirs, whose water availability is liable to be reduced by siltation and sediment-related pollution. The goal of this research was to evaluate the potential of multi-temporal high-resolution satellite imagery (RapidEye) to assess the suspended sediment concentration (SSC) in the medium-sized intermittent Jaguaribe River, Brazil, during a 5-year period. We validated 15 one-, two- and three-band indices for SSC estimation based on RapidEye spectral bands deduced in the context of the present investigation and nine indices proposed in the literature for other optical sensors, by comparing them with in-situ concentration data. The in-situ SSC data ranged from 67 $mg.L^{-1}$ to 230 $mg.L^{-1}$. We concluded that RapidEye images can assess moderate SSC of intermittent rivers, even when their discharge is low. The RapidEye indices performed better than those from literature. The spectral band that best represented SSC was the near infrared, whose performance improved when associated with the green band. This conclusion agrees with literature findings for diverse sedimentological contexts. The three-band spectral indices performed worse than those with only one or two spectral bands, showing that the use of a third band did not enhance the model ability. Besides, we show that the hydrological characteristics of semi-arid intermittent rivers generate difficulties to monitor SSC using optical satellite remote sensing, such as time-concentrated sediment yield; and its association with recent rainfall events and, therefore, with cloudy sky.

1. Introduction

Rivers are the major receptors and transporters of sediment from soil erosion; however, in most watercourses of the globe, sediment information is not readily available due to lack of monitoring (Syvitski et al., 2000), which becomes more critical in regions where rivers are intermittent and the annual sediment load is conveyed in a short period of time (Mano et al., 2009; Medeiros et al., 2014). Generally, the monitoring of sediment processes involves in situ observations at specific cross-sections, which cannot provide a broader spatial view of the processes in locations other than the monitoring spot. This limitation can result in inaccurate sediment-dynamic characterization (Liu et al., 2013). That is particularly serious because sediment transport in rivers may severely affect water policy, e.g., by reducing water availability due to reservoir silting (de Araújo et al., 2006) and pollution (Coelho et al., 2017). The Brazilian Semiarid Region is an extensive area (almost one million km^2), whose rivers are intermittent – with few exceptions – and whose water supply relies strongly on surface reservoirs, which are vulnerable to sediment dynamics (Lima Neto et al., 2011; Zhang et al., 2018). The lack of *in-situ* spatially and temporally-varied data on sediment routing reduces the effectiveness of environmental policies. Hence, the use of accurate, spatially-extensive and affordable techniques, such as remote sensing, is expected to be of great value for the improvement of sediment-dynamic knowledge and, therefore, of the water policy, since, unlike traditional monitoring methods, satellite remote sensing allows to collect data for large areas on a frequent and

* Corresponding author.
E-mail addresses: jairosp10@gmail.com (F.J.S. Pereira), costacag@gmail.com (C.A.G. Costa), saskia.foerster@gfz-potsdam.de (S. Foerster), arlena.brosinsky@uni-potsdam.de, arlena.brosinsky@gfz-potsdam.de (A. Brosinsky), jcaraujo@ufc.br (J.C. de Araújo).

https://doi.org/10.1016/j.jag.2019.02.009
Received 30 August 2018; Received in revised form 21 December 2018; Accepted 15 February 2019
Available online 21 March 2019

regular basis.

Previous studies have shown the feasibility of complementing both hydrological and sedimentological monitoring networks using satellite imagery (Martinez et al., 2009; Villar et al., 2012; Coelho et al., 2017; Zhang et al., 2018) because of its wide spatial coverage, high temporal resolution, and potential use as sediment concentration proxy (Ouillon et al., 2004; Binding et al., 2005). More specifically, some authors have reported a positive correlation that exists between the suspended sediment concentration (SSC) in rivers and their respective spectral response (Doxaran et al., 2002; Zhou et al., 2006; Chen et al., 2007). In fact, the amount of sediment in the water directly affects the reflectance of the solar radiation in the visible and near infrared portions of the spectrum: in general, the higher the suspended sediment concentration, the higher the surface water reflectance (Ritchie et al., 2003). Mertes et al. (1993) studied the Amazon River using Landsat images and demonstrated that satellite data can be used to estimate SSC accurately; whereas Martinez et al. (2004) confirmed the correlation of sediment concentration with satellite reflectance data using the MERIS and MODIS sensors. J.J. Wang et al. (2009b), investigating the Yangtze River, concluded that Landsat ETM + images are an acceptable proxy of SSC. However, satellite image analysis is limited by the spatial resolution of the images in relation to the width of the river. To avoid mixed spectral information, the river width should be larger than the pixel size (Wackerman et al., 2017). With pixel sizes of 30 m (e.g. Landsat) to 250–1000 m (e.g. MODIS), most optical satellite imagery is too coarse for monitoring intermittent rivers of small and variable width (typically ranging from 10 to 200 m), as is the case of the rivers located in the Brazilian Semiarid Region. Therefore, the overall objective of this work is to evaluate the potential of multi-temporal spatially high-resolution satellite imagery (RapidEye) for estimating the suspended sediment concentration in the medium-sized intermittent Upper Jaguaribe River. More specifically, the applicability of previously published SSC indices to RapidEye imagery is tested, and a set of new empirical indices that estimate SSC as a function of the spectral response of the waters of the Upper Jaguaribe River is evaluated using in-situ concentration data.

2. Material and methods

2.1. Study area

The Jaguaribe River Basin is inserted in the Caatinga, a tropical biome uniquely found in the northeast of Brazil, whose climate is hot semi-arid, with average annual temperature of 28 °C and precipitation typically ranging from 600 to 800 mm.yr^{-1}, concentrated from January to May, with marked irregularity in time and space (Santos et al., 2017). The Caatinga, whose name means 'white forest', in the native idiom, composes 12% of the Brazilian territory (800,000 km^2) and is characterized by leaf shedding of a large variety of both herbaceous and arborescent vegetation. The potential evaporation is three-fold the precipitation (2,000–2,400 mm.yr^{-1}), whereas the real evapotranspiration encompasses 75% of annual rainfall. The crystalline basement composes 85% of the Upper Jaguaribe River Basin; the soils, mostly Luvisols, are shallow, with medium to high fertility (Pinheiro et al., 2016; Coelho et al., 2018). Due to its large population (over 25 million inhabitants) and its water scarcity, the water supply in the biome has been met by thousands of dams. The focus area of this study is the Upper Jaguaribe River Basin (see Fig. 1), which drains an area of 24,538 km^2, and is controlled by the large Orós reservoir (1.94 billion cubic meters). Upstream the Orós dam, there are almost 5000 small (typically 0.5 hm^3) and middle-sized reservoirs (up to 10 hm^3), which strongly influence water and sediment routing in the watershed (Peter et al., 2014; de Araújo and Bronstert, 2016). The river section analysed in this study is 30 to 250 m wide, located in the city of Iguatu (approximately 325 km from the river source). We selected because this section, immediately upstream the large Orós dam, because it coincides with the location where authorities have monitored water and sediment discharges for several decades.

2.2. In-situ data

The mean daily *in-situ* SSC equals the ratio between the sediment load (QSS) and the river discharge (Q), which is measured daily (ANA, 2017). The sediment load is given by the rating curve (Eq. (1)), developed by Lima Neto et al. (2011) for the Iguatu section, based on 40 field measurements performed between 2003 and 2009. In the analysis, an important variable is the precipitation of the five previous days (PP, see Table 1). Daily-average basin precipitation data is available at FUNCEME (2018), based on a network of 90 gauges and computed using the Thiessen-polygon method.

$$Q_{SS}(\text{Mg. day}^{-1}) = 5.031.\ Q(\text{m}^3.\ \text{s}^{-1})^{1.346} \quad (1)$$

2.3. Satellite data

From July 2009 to May 2014, a total of 64 high-resolution RapidEye satellite images were acquired, taken simultaneously with in-situ SSC data. However, only twelve images representing different discharge and SSC conditions could be used (Fig. 2), i.e., 81% of the set were discarded, mainly due to three reasons: (i) 29 images (56% of the rejected ones) were from the dry season (July–December), when the river was not flowing; (ii) 18 (34%) were from the rainy season, but because of the multi-annual drought (2012–2016: see de Araújo and Bronstert, 2016), there was no discharge in the river; and (iii) six (10%) were discarded due to excessive cloudiness. Additionally, because of the drought, there were few high-discharge events in the last three years of the study period, resulting in a limited number of events with simultaneous measurable discharges and useful images in the 59-month study period. The combination of few discharge events often coinciding with cloudy conditions poses a great challenge for remote sensing to monitor intermittent rivers.

The RapidEye imagery has five bands in the VNIR range: blue (440–510 nm), green (520–590 nm), red (630–685 nm), red edge (690–730 nm) and near-infrared (NIR, 760–850 nm). Orthorectified Level 3 A imagery with a spatial resolution of 5 m was obtained (RapidEye, 2015) and subsequently atmospheric corrections of the images were performed using the 6S (Second Simulation of Satellite Signal in the Solar Spectrum) model (Antunes et al., 2012; Bonansea et al., 2015), originally developed to simulate radiance at the satellite level (Vermote et al., 1997). Clouds in the images were masked manually before further analyses. The selected Iguatu cross section encompasses several RapidEye pixels due to the high spatial resolution (5 m) of the images and the river width (typically 20 m – 60 m during acquisition of the available images). At the first step, we selected 21 transverse pixels of the Iguatu cross section, where measurements of water discharge and sediment load have been made for several decades: one in the center of the riverbed, and ten pixels at each side. Then, we analyzed each pixel individually to check if it really contained water, considering that water has a much lower reflectance than the terrestrial surfaces. The central pixel is associated with the number zero, with negative-numbered pixels to its left and positive-numbered pixels to its right (Fig. 1). When it was not possible to analyze the data in the exact Iguatu section due to the presence of clouds or macrophytes (Zhang et al., 2018), a cross section as close as possible to the original one was selected (upstream, maximum 100 m). The macrophytes were visually detected, according to the spectral response of the pixel.

In order to assess the applicability of RapidEye imagery for SSC monitoring in intermittent rivers, we analyzed the performance of 24 indices that correlate SSC with reflectance values in the Jaguaribe River, which consisted of two groups: (a) nine existing indices from the literature; and (b) fifteen indices generated in the context of the present investigation that used one (SSB), two (DSB), and three (TSB) bands

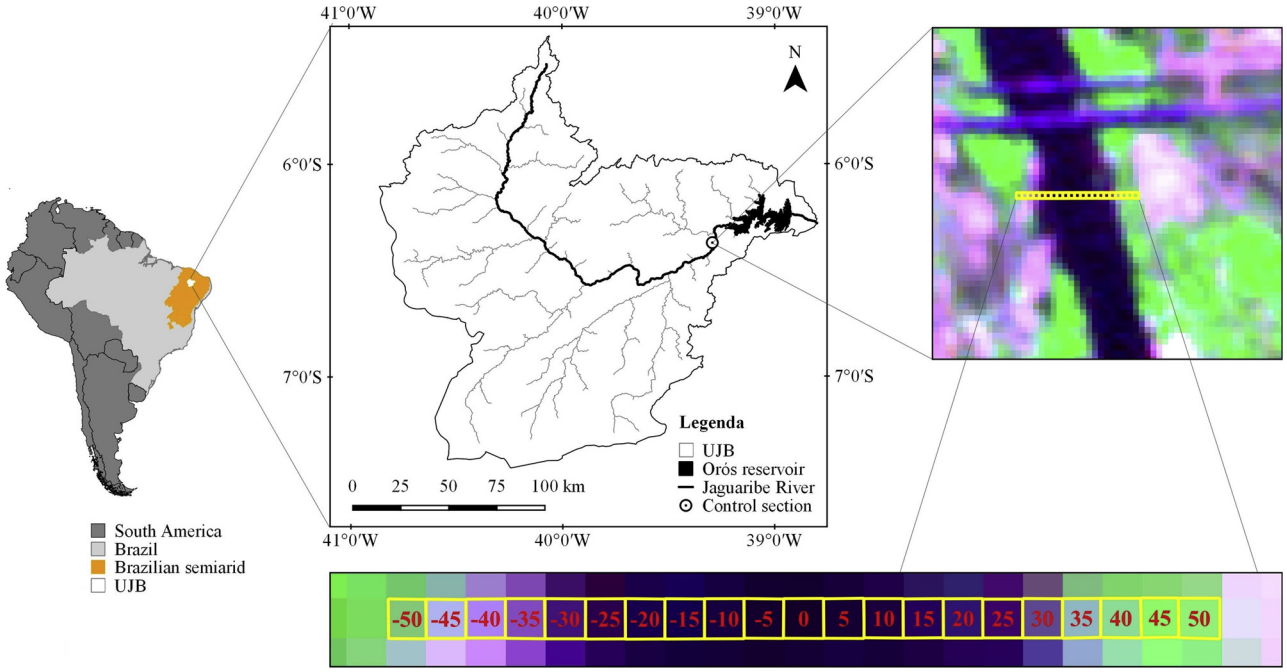

Fig. 1. Location of the Upper Jaguaribe Basin (UJB); the Iguatu river section; the Orós reservoir; and Rapideye image pixels along the analyzed cross section (spatial resolution of 5 m, numbers indicate distance in meters from the center pixel).

Table 1
Dates of image acquisition, precipitation of five previous days (PP), river discharge (Q), suspended sediment concentration (*in-situ* SSC) and reflectance of spectral bands of the center pixel (RapidEye) in the Jaguaribe River (Iguatu section): band 1 (blue: 440–510 nm); band 2 (green: 520–590 nm); band 3 (red: 630–680 nm); band 4 (red edge: 690–730 nm); and band 5 (NIR: 760–850 nm). The events are presented in decreasing order of SSC, the criterion to separate 'calibration' from 'validation' events.

Event date	PP (mm)	Q ($m^3.s^{-1}$)	SSC ($mg.L^{-1}$)	Reflectance of the RapidEye image (%)				
				Band 1	Band 2	Band 3	Band 4	Band 5
Events used for calibration								
30/03/2011	27	44.83	217	9.56	13.67	17.47	18.57	18.84
07/03/2011	29	23.71	174	4.95	9.01	11.53	11.09	7.44
21/03/2011	9	6.89	114	6.18	8.88	8.54	7.87	6.64
31/03/2014	34	3.79	92	4.72	7.86	7.25	6.56	5.82
27/06/2011	1	2.07	75	1.19	2.56	1.63	3.22	2.73
26/05/2014	6	1.47	67	1.06	2.22	2.53	4.09	3.53
Events used for validation								
20/04/2010	31	52.75	230	5.12	8.77	11.26	10.86	9.12
21/05/2011	35	42.83	214	4.16	7.84	9.14	9.21	8.51
11/04/2011	30	10.63	132	6.23	10.92	13.54	12.91	11.78
25/04/2012	8	4.00	94	2.76	5.15	4.76	4.69	5.56
18/05/2010	18	2.35	78	3.75	6.20	6.70	5.67	4.34
18/07/2009	1	1.69	70	3.21	4.87	2.18	2.29	3.09

(Table 2). The nine indices proposed in the literature were developed based on data from different sensors. Table 3 shows the wavelength ranges of the spectral bands used and the spatial resolution of the sensors including RapidEye for reference purposes. The RapidEye indices were generated by the LABFit software (Silva et al., 2004), applying the Levenberg-Marquardt optimization algorithm (Levenberg, 1944; Marquardt, 1963), also known as *damped least-squares*. The best-fit relations between the in-situ SSC of the central pixel (pixel zero) and the spectral reflectance of individual or a combination of bands were obtained based on the LABFit library that provides approximately 500 predefined non-linear regression functions. From the twelve selected events, six were employed for calibration (of the 15 indices derived in this research) and the remaining six for validation of the 24 indices. We hierarchized the events represented in the images in terms of SSC magnitude, and used the odd-numbered ones for validation and the even-numbered ones for calibration (Table 1). The performance parameters were the determination coefficient (R2); the mean absolute error (MAE, Eq. (2)); the root of the mean square error (RMSE, Eq. (3)); and the Nash-Sutcliffe coefficient (NSE, Eq. (4)). In Eqs. (2)–(4), C_m refers to measured SSC; C_C to computed SSC; $\bar{C_m}$ to the average measured SSC; and N to the sample size.

$$MAE = \frac{1}{N}.\sum_{1}^{N}|C_m - C_c| \quad (2)$$

$$RMSE = \sqrt{\frac{1}{N}\sum_{1}^{N}(C_m - C_c)^2} \quad (3)$$

$$NSE = 1 - \frac{\sum(C_m - C_c)^2}{\sum(C_m - \bar{C_m})^2} \quad (4)$$

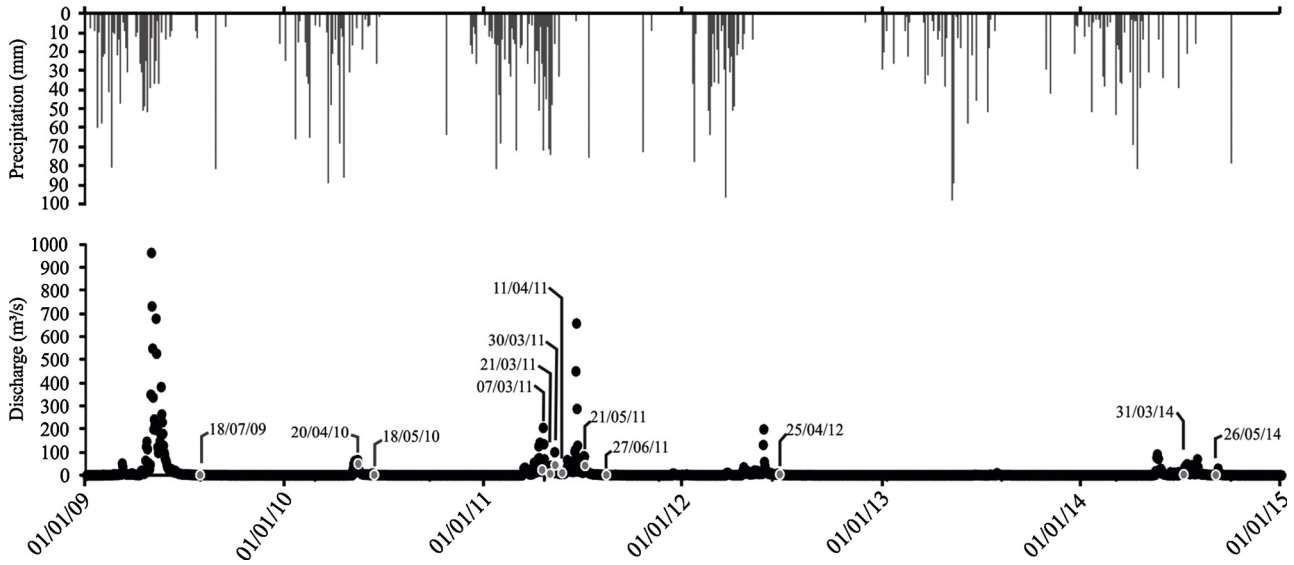

Fig. 2. Temporal evolution (2009–2014) of precipitation (grey lines on top), river discharges (black dots) and dates of analysis, when both SSC and good-quality satellite imagery were available, shown in grey dots in the lower axis (For interpretation of the references to colour in this figure legend, the reader is referred to the web version of this article).

Table 2
Indices that relate suspended sediment concentration (SSC, mg L^{-1}) with reflectance (ρ, %). In part (a) of the table, the indices (1–9) are derived from literature, whereas the indices of part (b) (SSB, DSB, TSB) were established in this work. The Nash-Sutcliffe coefficient (NSE) refers to SSC data from the intermittent Jaguaribe River.

(a)					
Index ID	SSC range (mg.L^{-1})	Satellite	Index	Nash-Sutcliffe coefficient (NSE)	
				Calibration / Source	Validation
1	100–1,000	LANDSAT	$\ln(SSC) = -6.2*\left(\frac{\rho red}{\rho nir}\right) + 1.4*\left(\frac{\rho red}{\rho nir}\right)^2 + 10.8$	Topliss et al. (1990)	−14.31
2	17–2,500	MODIS	$\ln(SSC) = (43.233*\rho nir) + 1.396$	Wang et al. (2009a)	−2.27
3	< 2000	CASI	$SSC = 529*\rho nir$	Wass et al.(1997)	−2.23
4	7–1,150	LANDSAT	$SSC = (69.39*\rho red) - 201$	Islam et al. (2001)	−22.89
5	2–168	LANDSAT	$\ln(SSC) = -9.21*\left(\frac{\rho green}{\rho red}\right) + 2.71*\left(\frac{\rho green}{\rho red}\right)^2 + 8.45$	Ritchie and Cooper (1991)	−3.77
6	100–1,000	MOS/MESSR	$\ln(SSC) = -4.8*\left(\frac{\rho green}{\rho red}\right) + 0.9*\left(\frac{\rho green}{\rho red}\right)^2 + 10.4$	Topliss et al. (1990)	−159.51
7	17–2,500	MODIS	$\ln(SSC) = (50.171*\rho red) + 1.523$	Wang et al. (2009a)	−24.80
8	1–500	MODIS	ρ red= 7.5*log(CSS) + 1.6	Chu et al. (2009)	−3.65
9	22–2,610	LANDSAT	$\ln(SSC) = 3.18236*\ln(\rho nir) - 1.40060$	Wang et al. (2009b)	−9.77
(b)					
SSB1[a]	67–230	RapidEye	$SSC = 62.56*EXP[0.13*\rho blue]$	0.76	0.04
SSB2	67–230	RapidEye	$SSC = 0.94*[\rho green]^2 + 51.70$	0.94	0.07
SSB3	67–230	RapidEye	$SSC = 62.68*1.08^{\rho red}$	0.93	0.30
SSB4	67–230	RapidEye	$SSC = 18.49*[\rho red\ edge] - 0.36*[\rho red\ edge]^2$	0.95	0.44
SSB5	67–230	RapidEye	$SSC = 23.65*[\rho nir] - 0.64*[\rho nir]^2$	0.88	**0.54**
DSB1[a]	67–230	RapidEye	$SSC = 16.88*[\rho red\ edge] - 0.27*[\rho nir]^2$	0.96	0.41
DSB2	67–230	RapidEye	$SSC = \frac{[\rho red]}{0.0589 + 0.0012*[\rho nir]}$	0.80	0.35
DSB3	67–230	RapidEye	$SSC = \frac{[\rho nir]}{0.03909 + 0.00023*[\rho green]^2}$	0.83	**0.58**
DSB4	67–230	RapidEye	$SSC = 19.49*[\rho red\ edge] - 0.46*[\rho red]^2$	0.95	0.47
DSB5	67–230	RapidEye	$SSC = \frac{[\rho red\ edge]}{0.05306 + 0.00017*[\rho green]^2}$	0.97	0.51
DSB6	67–230	RapidEye	$SSC = 74*[\rho green]^{0.02446*[\rho red]}$	0.90	0.21
TSB1[a]	67–230	RapidEye	$SSC = 32.29*\left(\frac{[\rho nir] + [\rho red\ edge] + [\rho red]}{3}\right)^{0.6613}$	0.92	**0.44**
TSB2	67–230	RapidEye	$SSC = 10{,}209.\xi^{-1}.EXP(-16.55/\xi)$; $\xi = [\rho nir].[\rho red\ edge]/[\rho red]$	0.87	0.40
TSB3	67–230	RapidEye	$SSC = 46.46*\left([\rho nir]*\frac{[\rho red]}{[\rho red\ edge]}\right)^{0.531}$	0.82	0.43
TSB4	67–230	RapidEye	$SSC = 0.433*\left(\frac{[\rho red\ edge]*[\rho red]}{[\rho nir]}\right)^2 + 67.19$	0.95	0.22

[a] SSB refers to one-band indices, DSB to two-band indices, and TSB to three-band indices.

Table 3
Spectral band ranges and spatial resolution of the sensors used in the derivation of the nine published SSC indices that were tested in this study (for references to the published indices see Table 2).

Sensor	Wavelength bands (nanometers)					Spatial Resolution (m)
	Blue	Green	Red	Red-edge	NIR	
MODIS	459–479	545–565	620–670	–	841–876	250,500 and 1000
MOS – MESSR		510–590	610–690	–	720–800 800–1100	50
CASI (airborne)	402.5–421.8 453.4–469.2	531.1–543.5 571.9–584.3	630.7–643.2 666.5–673.7	–	736.6–752.8 776.3–785.4	1
Landsat 4-5 –MSS and TM	450–520	520–600	630–690	–	760–900	30
Landsat 7 – ETM +	450–520	520–600	630–690	–	770–900	30
Landsat 8 – OLI	452–512	533–590	636–673	–	851–879	30
RapidEye	440k510	520–590	630–685	690–730	760–850	5

3. Results

3.1. In-situ data

Table 1 presents the data of the twelve events used in the analysis. According to the in-situ data, SSC in the Upper Jaguaribe River was low to moderate, ranging from 67 $mg.L^{-1}$ to 230 $mg.L^{-1}$. Measured discharges of the events analyzed did not surpass 53 $m^3.s^{-1}$ (Table 1) although two floods with peaks of 650 $m^3.s^{-1}$ and 200 $m^3.s^{-1}$ occurred in the study period (May 2011 and April 2012, respectively). These events could not be included in the analysis due to the high cloudiness of imagery. Six of the twelve available RapidEye images were acquired in 2011, a year in which also most of the relatively high SSC values were measured (Table 1). In fact, 2011 presented above-average precipitation (1651 mm: FUNCEME, 2018) and the most intense precipitation events during the study period, which justifies the occurrence of relatively high sediment loads. In 2012, there was the onset of a multi-annual drought (de Araújo and Bronstert, 2016), with a marked decrease in precipitation, runoff, and consequently sediment load (visible from Fig. 2).

3.2. Satellite data

Table 2 presents the performance (NSE) of the 24 indices relating SSC and spectral reflectance for the Jaguaribe River section. Additionally, Fig. 3 presents the performance (R^2, MAE, RMSE, NSE) of all indices graphically. None of the literature formulations could represent the SSC data in the intermittent Jaguaribe River: they all generated negative NSE values and excessively high error measures (Table 2, Fig. 3). The error estimates of the literature indices are extremely high (maximum MAE = 705 $mg.L^{-1}$, maximum RMSE = 805 $mg.L^{-1}$), whereas the errors of the indices derived in this study are one order of magnitude lower (maximum MAE = 48 $mg.L^{-1}$; maximum REMQ = 63 $mg.L^{-1}$). The RapidEye-based indices had an outstanding NSE in the calibration process, with an average of 0.90. However, the NSE in the validation process was considerably lower (0.36 on average). From the indices developed for one band (SSB), the one that performed best (highest NSE) was SSB5, which relates the SSC with the near infrared reflectance. Among the two-band indices (DSB), those that employed the short wavelength band 1 (blue, 440–510 nm) did not achieve minimally acceptable results and, therefore, were excluded from Table 2. The best result for the combination of two bands was that of index DSB3, which relates SSC with the reflectance of a short and a long wavelength band (green band 2 and near infrared band 5, respectively). Other indices (e.g., DSB1, DSB4 and DSB5) also achieved good responses as SSC proxies, with moderate coefficient of determination (R^2 ~ 0.6) and NSE (~0.5), as shown in Fig. 3. In general, one depicts that, for the RapidEye images, the longest wavelength bands (red edge and near

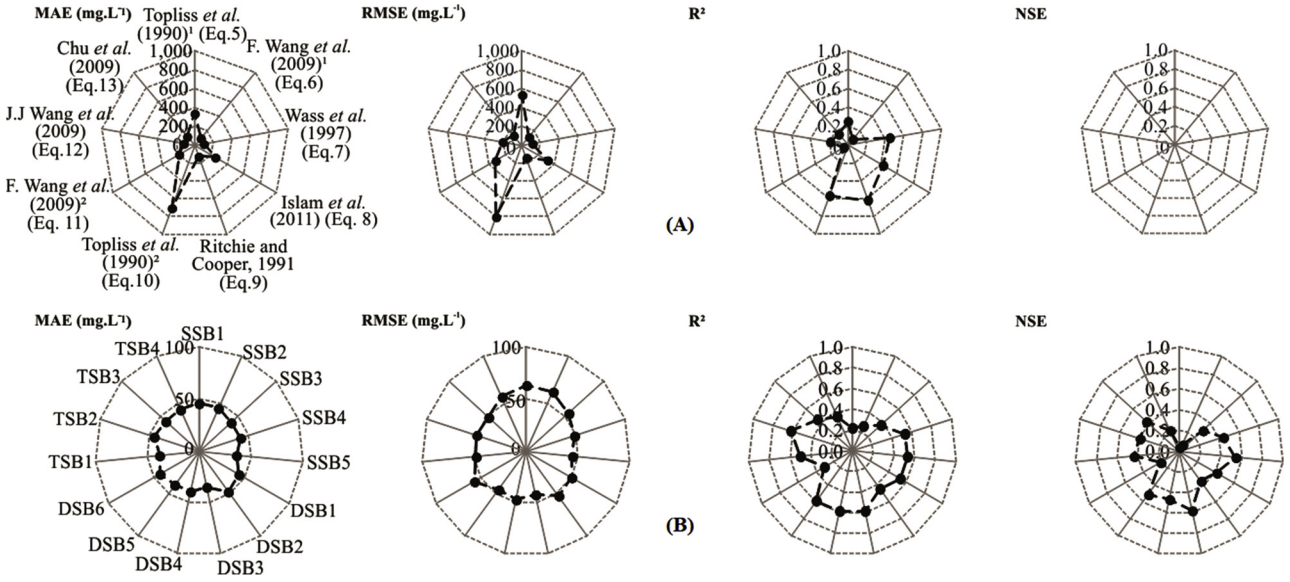

Fig. 3. Performance of (A) nine literature; and (B) 15 Rapid-Eye indices that relate SSC with spectral reflectance (Table 2) for six events (validation) in the intermittent Jaguaribe River (Table 1), using the following parameters: mean absolute error (MAE); root mean square error (RMSE); coefficient of determination (R^2); and Nash-Sutcliffe coefficient (NSE). The NSE upper graphic is empty because all Literature indices provided negative NSE values (in this specific graphic, the scale goes from zero to one).

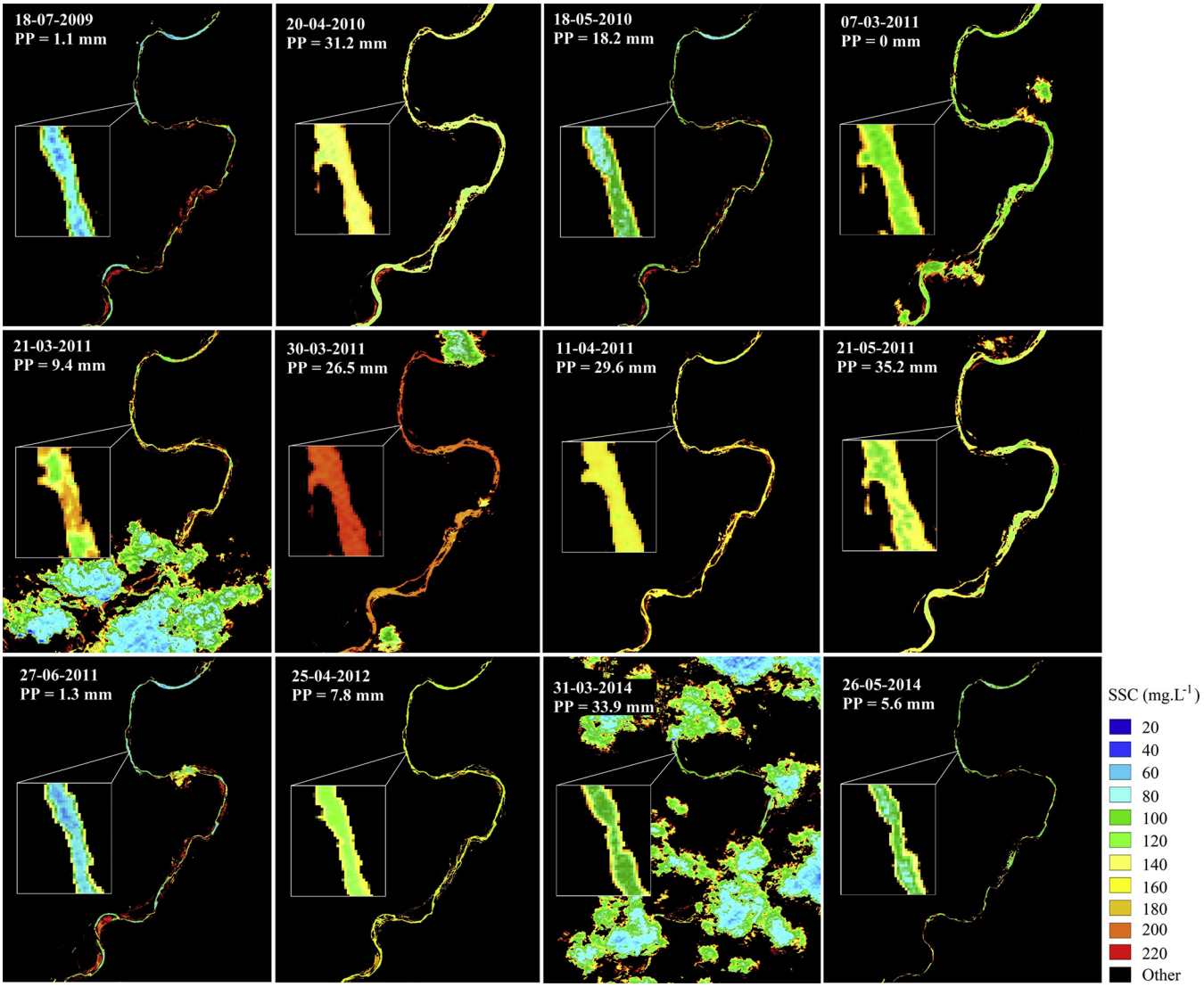

Fig. 4. Five-day previous precipitation (PP) and spatial distribution of suspended sediment concentration (SSC) in the Jaguaribe River, estimated by Index DSB3 (Table 2).

infrared) compose all good-performance formulations, not only in two-band (DSB1, DSB3, DSB4, DSB5), but also in one-band (SSB5) and three-band (TSB1) spectral indices. Contrarily, short wavelength bands are limited in representing SSC: band 1 (blue) seems inadequate for this purpose, whereas band 2 (green) can be helpful, as long as it is combined with a long wavelength band (e.g., DSB3 and DSB5). According to Table 2, the best index considering three spectral bands (3 red, 4 red-edge, and 5 NIR) was TSB1. Fig. 4 shows a spatially variable SSC plot of a Jaguaribe River reach during the 12 events, estimated by the best-performing (DSB3) index, with the respective 5-day previous precipitation. The plots show that, due to the RapidEye pixel size of 5 m, it is possible to trace concentration spatial distribution even in an intermittent river, such as the Jaguaribe, during low-discharge periods.

4. Discussion

4.1. In-situ data

One factor influencing the SSC behavior is the geological characteristic of its basin. Because it is mostly (85%) composed of crystalline bedrock the UJB has limited groundwater storage capacity, which contributes to the increase in discharge following intensive precipitation events, favoring the rapid and efficient loading of materials to the rivers. However, Medeiros et al. (2014) have shown that the sediment routing in the Brazilian semiarid region is strongly disconnected, and high loads should only be expected during storms. Another feature that is strongly associated with the generally moderate SSC concentration in the intermittent Jaguaribe River is the dense network of dams in the watershed, which causes sediment trapping. In fact, Lima Neto et al. (2011) state that, in the UJB, small and middle-sized dams are responsible for the retention of 52% of the total sediment yield, reducing the SSC in the early rainy season (usually the first three months of the year). Should the rainy season continue for a longer period, and/or an extreme event happen, flood avalanches will occur (Peter et al., 2014), silted material will be remobilized and SSC tends to augment considerably, causing the propagation of peaks of sediment to the basin outlet (Lima Neto et al., 2011; Medeiros et al., 2014). This phenomenon has not happened in any of the monitored events in the context of this work, which partially explains the moderate SSC values. The concentration time of a watershed, which is the duration of the water transfer from the furthest point in the basin to its outlet, is 4.3 days in the study catchment area. The fact that the previous rainfall duration (5 days) is close to the concentration time of the watershed (4.3 days) is a strong indication that the sediment mobilization occurs

primarily at the hillslopes, rather than at the river bed, which agrees with Lima Neto et al. (2011) and Medeiros et al. (2014).

4.2. Satellite data

The best-fit literature index (Wass et al., 1997: lowest mean absolute error MAE = 99 mg.L^{-1}; and highest NSE -2.23) was generated for British rivers, using spatially high-resolution airborne Compact Airborne Spectrographic Imager (CASI) imagery and considering a wide range of turbidity. These might be the reasons for its relatively good performance in the Jaguaribe River, if compared to the other indices. At the opposite extreme, the indices deduced for Fundy Bay and Mackenzie River (Topliss et al., 1990), located in low-temperature regions on the Atlantic coast of North America, performed poorly using MOS-MESSR imagery. They yielded high absolute error (threefold the measured concentration: MAE up to 705 mg.L^{-1}) and NSE as low as -160. Besides the climatic inequality, there are other relevant differences between the regions (cold wet North America and hot dry South America), such as the high SSC of their samples; the high amplitude of the tides (Desplanque and Mossman, 2001); the type of material present in the water, mainly due to the influence of the North Atlantic Sea; as well as the images used and their processing method. The poor performance of all selected literature indices (based on measured in-river SSC) calls for the fact that the state-of-the-art remote sensing has limited potential to extrapolation, both in terms of application site and optical sensors. The retrieval of SSC from remotely sensed images is limited by the spatial, temporal, and spectral resolutions of the sensors (Imen et al., 2015) In this regard; Dorji and Fearns (2017) studied the impact of the spatial resolution of satellite sensors in the suspended sediment concentration in Australia and concluded that different sensors with different spatial resolutions alter the results. Ody et al. (2016) showed that, in the Gulf of Lion, France, and the variability of the suspended sediment concentration at the turbid fronts and edges of the river plume increased with the decrease of spatial image resolution. The results based on the literature indices show that Landsat (30 m) and MODIS (250–1000 m) indices have similar behavior when applied to Jaguaribe River.

Lodhi et al. (1998) stated that, between 700 and 900 nm, the reflectance increases more uniformly with increasing SSC than in the region of 400 to 700 nm and that the near-infrared region seems to be the most useful for estimating SSC in water. In a study by Wang et al. (2010), the reflectance of the bands 3 (459–479 nm), 4 (545–565 nm) and 1 (620–670 nm) of the MODIS sensor, showed a positive relationship with SSC, but the increase in reflectance with the increase of SSC became significantly slower when SSC surpassed 150 mg.L^{-1}. The same behavior was observed for the RapidEye images, as can be depicted from Fig. 5 (bands 1 and 2). It indicates that the reflectance of the shortest wavelength bands (1, blue; and 2, green) increases with SSC for low concentration values. However, when SSC surpasses 100 mg.L^{-1}, reflectance does not vary accordingly, ranging typically from 5% to 10% (blue band) and 8% to 14% (green band), which points out to a saturation process or an overall low signal-to-noise ratio of the shorter wavelength bands. Differently, for the remaining bands, the spectral response is sensitive for the whole concentration spectrum. This explains, at least partially, why the short wavelength bands 1 and 2 (blue and green, respectively) performed worse than the other bands. Wackerman et al. (2017), examining the SSC in the Mekong River, suggested the division of the data into two ranges to achieve better linear indices. The authors divided the SSC values below and above 70 mg.L^{-1}, improving their results (see also Dorji et al., 2016). Another way to improve SSC results is using neural network regression methods that have potential to surpass traditional techniques of remote sensing data analysis (Mas and Flores, 2008; Peterson et al., 2018). Neural network have been applied and considered a viable option for sedimentological research (Adib and Jahanbakhshan, 2013); Sari et al. (2017) experimented artificial neural networks to estimate SSC in Taboão River (Brazil) with limited data, and emphasized the importance of this new methodology. Ouillon et al. (2004) and Binding et al. (2005) appointed several bands of the visible and the near infrared (NIR) range as possible proxies of SSC, which is in agreement with the results in the Jaguaribe River. Long and Pavelsky (2013) called the attention to the prevalence of long wavelength bands (near infrared and red) as SSC predictors, as also detected in the present investigation. However, the authors also state that some of the top indices combined near infrared bands with a green or blue band, implying that short wavelength bands may be useful in detecting sediment concentration, as long as they are interconnected with a near infrared band. This statement agrees with the result by Wackerman et al. (2017), which shows that the best index was a function of the NIR/green ratio, which provided higher correlation and lower RMSE than the index using the red band. These findings are in full agreement with our work: the best performing models were those with either red, red edge or near infrared bands. Notwithstanding the poor performance of the green band for one-band indices, it composes the best-fit index (DSB3), together with the NIR band. The analysis of the best RapidEye-based model for different numbers of bands shows an improvement when, instead of only one (SSB5, validation NSE = 0.54, ratio between validation and calibration NSE = 0.61), two bands were used (DSB3, validation NSE = 0.58, ratio between validation and calibration NSE = 0.70). This means that the inclusion of the green band reflectance added relevant information. However, when we added a third band, the best-fit model clearly deteriorated (TSB1, validation NSE = 0.44, ratio between validation and calibration NSE = 0.48), indicating that the addition of more data did not result in the improvement of information.

Satellite imagery offers a wide spatial coverage (Martinez et al., 2009; Villar et al., 2012; Coelho et al., 2017; Zhang et al., 2018) and has been shown to be useful for estimating SSC by several authors (Ouillon et al., 2004; Binding et al., 2005). However, the poor performance of indices from remote sensing literature and the moderate validation NSE of the RapidEye-based indices (when compared to the high calibration NSE) indicate that there are important challenges to face, especially for intermittent rivers. In the Brazilian semiarid region, where most rivers are intermittent (even those with catchment areas as large as 10^5 km^2), baseflow discharges are usually negligible and Hortonian runoff prevails, causing river discharges to be mainly composed of hillslope surface runoff (Santos et al., 2017). Despite the low river discharges, the cloud coverage in the focus region is high during the rainy season, which enhances the obstacles to perform spectral analysis of orbital images (Fig. 4). We have investigated if there was any valid correlation between *in-situ* SSC and rainfall for several durations, and observed a good positive correlation between SSC and the five-day antecedent precipitation (PP). Considering all (12) valid images, the relation SSC versus PP yielded $R^2 = 0.58$. However, if one cloudy image (31 March 2014, see Fig. 4) is discarded, the correlation increases considerably ($R^2 = 0.78$). Consequently, the most relevant sediment loads occur, due to widespread sediment remobilization, during high-discharge events, which are inevitably associated with recent precipitation events. This simultaneity of relevant sediment load and intensive cloudiness in intermittent rivers brings, therefore, a major obstacle to the application of remote sensing to assess SSC. Another consequence of the hydrological features of intermittent rivers is that only few events are able to generate flow avalanches (Peter et al., 2014). In fact, Lima Neto et al. (2011) concluded that only one semester (in 2004) contributed with 83% of the total sediment load in the UJB for a period of 25 years (1984–2008). This means that, either due to the excessive presence of clouds or to unavailability of images, and the acuteness of sediment routing in these areas, remote sensing techniques may fail to register the events that can cause outstanding impacts on regional geomorphology.

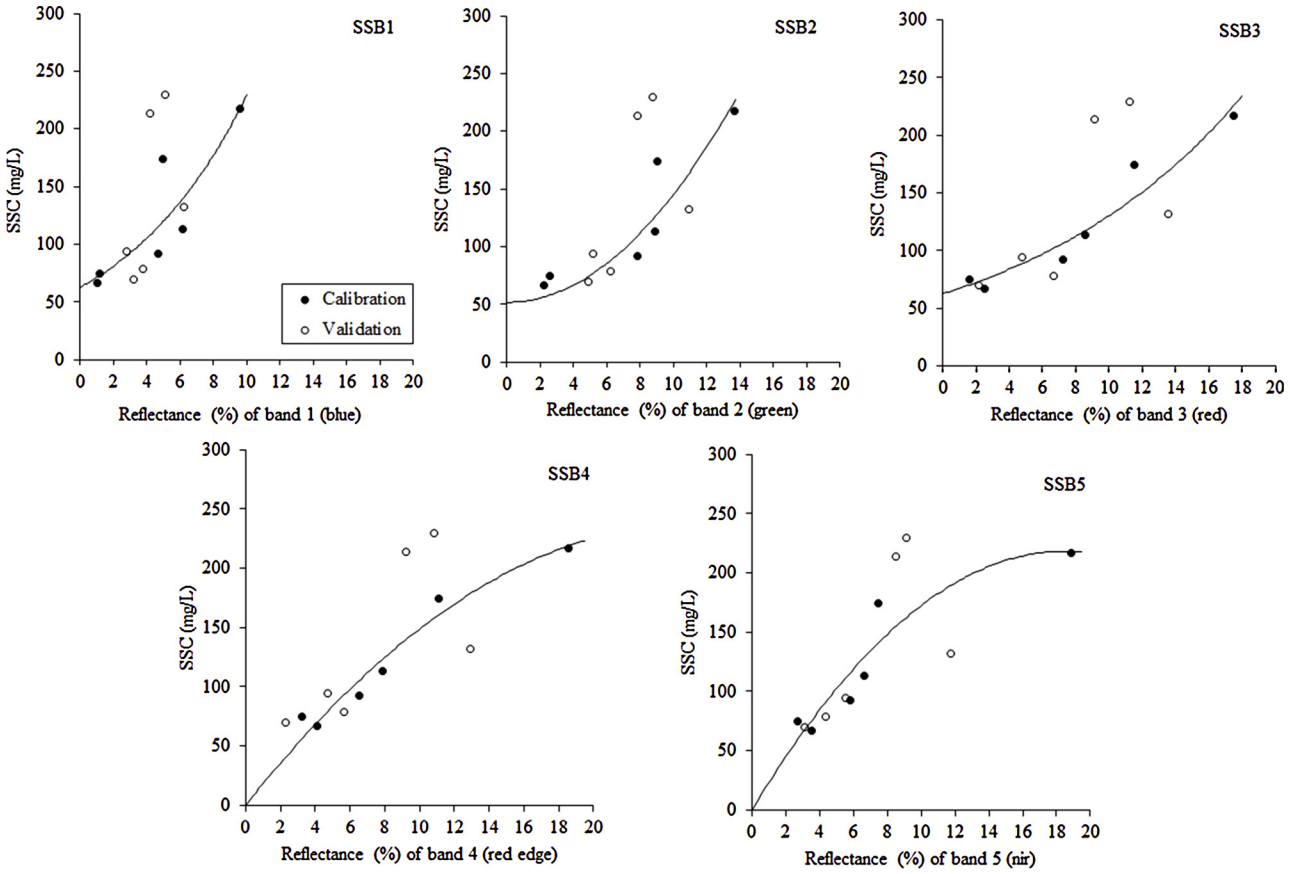

Fig. 5. Relation between reflectance for the five spectral bands of RapidEye images (Equations SSB, see Table 2) and suspended sediment concentration (SSC) for the period from 2009 to 2014 in the Jaguaribe River (Iguatu section).

5. Conclusions

The results of this investigation show that images of the RapidEye satellite constellation can assess moderate (67–230 mg.L^{-1}) suspended sediment concentration (SSC) of an intermittent river, even when the discharge is low (2 m^3.s^{-1}). The here-proposed RapidEye indices performed better for the intermittent Jaguaribe River than those proposed in the literature, which used other optical sensors with different spatial, spectral and temporal resolutions. In general, the spectral band of the RapidEye satellite constellation that best represented SSC in the intermittent Jaguaribe River was that of the longest wavelength (band 5, NIR, 760–850 nm). The NIR band composes the three best-performing RapidEye-based indices, using one (SSB), two (DSB) and three (TSB) spectral bands. The index that provided the best result in this work was DSB3, composed by an association of green (520–590 nm) and near infrared (760–850 nm) bands, which agrees with the conclusion by Long and Pavelsky (2013) that the combination of green and NIR bands yields good predictors for SSC. It is noteworthy that the authors *op cit.* studied wetland waters with high sediment concentration (up to 3602 mg.L^{-1}), whereas the Jaguaribe River dataset presented only moderate SSC. The three-band spectral indices (TSD) performed worse than those with only one (SSB) or two (DSB) spectral bands, showing that the addition of data (a third band, in this case) does not necessarily enhance the model representativeness. Despite the promising results, the hydrological features of intermittent rivers impose some serious challenges to monitor SSC using remote sensing: sediment yield is highly concentrated in time, and simultaneous satellite imagery might not be available. Besides, high-yield events in intermittent rivers substantially depend on recent precipitation, which presupposes cloudy sky and, therefore, limited optical access. Additionally, in our study, the long-term drought that happened during the 59-month monitoring period minimized the number of events with simultaneous measurable discharges and useful satellite images. It is significant, therefore, to proceed with the validation of the indices resulting from this research for larger flows. Another relevant outlook would be to test the new multispectral Sentinel-2 image data, whose spatial resolution is 10 m, to assess suspended sediment concentration in intermittent rivers.

Acknowledgements

This research was supported by the PROBRAL Project (Grant n. 424/14), funded by the Brazilian Capes Foundation and by the German Academic Exchange Service – DAAD; as well as by the Brazilian Council for Scientific and Technological Development – CNPq (Grant n. 301677/2015-8). RapidEye satellite data were provided by the RapidEye Science Archive (RESA) of DLR with resources of the German Federal Ministry of Economic Affairs and Energy.

References

Adib, A., Jahanbakhshan, H., 2013. Stochastic approach to determination of suspended sediment concentration in tidal rivers by artificial neural network and genetic algorithm. Can. J. Civ. Eng. 40 (4), 299–312. https://doi.org/10.1139/cjce-2012-0373.

ANA, 2017. Agência Nacional De Águas (Accessed on July 10, 2017). http://www.snirh.gov.br/hidroweb/.

Antunes, M.A.H., Debiasi, P., Costa, A.R., Gleriani, J.M., 2012. Atmospheric correction of ALOS/AVNIR-2 images using the 6S model.". [In Portuguese.]. Revista Brasileira de Cartografia 64, 531–539.

Binding, C.E., Bowers, D.G., Mitchelson-Jacob, E.G., 2005. Estimating suspended sediment concentrations from ocean colour measurements in moderately turbid waters; the impact of variable particle scattering properties. Remote Sens. Environ. 94 (3), 373–383. https://doi.org/10.1016/j.rse.2004.11.002.

Bonansea, M., Ledesma, C., Rodríguez, C., Pinotti, L., Antunes, M.H., 2015. Effects of atmospheric correction of Landsat imagery on lake water clarity assessment. Adv. Space Res. 56 (11), 2345–2355. https://doi.org/10.1016/j.asr.2015.09.018.

Chen, Z., Hu, C., Müller-Karger, F., 2007. Monitoring turbidity in Tampa Bay using MODIS/Aqua 250-m imagery. Remote Sens. Environ. 109 (2), 207–220. https://doi.org/10.1016/j.rse.2006.12.019.
Coelho, C., Heim, B., Foerster, S., Brosinski, A., de Araújo, J.C., 2017. In-situ and satellite observation of CDOM and chlorophyll-a dynamics in small water surface reservoirs in the Brazilian semiarid region. Water 9 (913). https://doi.org/10.3390/w9120913.
Coelho, V.H.R., Bertrand, G.F., Montenegro, S.M.G.L., Paiva, A.L.R., Almeida, C.N., Galvão, C.O., Barbosa, L.R., Batista, L.F.D.R., Ferreira, E.L.G.A., 2018. Piezometric level and electrical conductivity spatiotemporal monitoring as an instrument to design further managed aquifer recharge strategies in a complex estuarial system under anthropogenic pressure. J. Environ. Manage. 209, 426–439. https://doi.org/10.1016/j.jenvman.2017.12.078.
De Araújo, J.C., Bronstert, A., 2016. A method to assess hydrological drought in semiarid environments and its application to the Jaguaribe River basin, Brazil. Water Int. 41, 213–230. https://doi.org/10.1080/02508060.2015.1113077.
De Araújo, J.C., Güntner, A., Bronstert, A., 2006. Loss of reservoir volume by sediment deposition and its impact on water availability in semiarid Brazil. Hydrological Sciences Journal des Sciences Hydrologiques 51 (1), 157–170. https://doi.org/10.1623/hysj.51.1.157.
Desplanque, C., Mossman, D.J., 2001. Bay of fundy tides. Geosci. Can. 28 (1).
Dorji, P., Fearns, P., 2017. Impact of the spatial resolution of satellite remote sensing sensors in the quantification of total suspended sediment concentration: a case study in turbid waters of Northern Western Australia. PLoS One 12 (4). https://doi.org/10.1371/journal.pone.0175042.
Dorji, P., Fearns, P., Broomhall, M., 2016. A semi-analytic model for estimating total suspended sediment concentration in turbid coastal waters of northern western Australia using MODIS-Aqua 250 m data. Remote Sens. 8 (7), 556. https://doi.org/10.3390/rs8070556.
Doxaran, D., Froidefond, J.M., Lavender, S., Castaing, P., 2002. Spectral signature of highly turbid waters: application with SPOT data to quantify suspended particulate matter concentrations. Remote Sens. Environ. 81 (1), 149–161. https://doi.org/10.1016/S0034-4257(01)00341-8.
FUNCEME, 2018. Ceará State Meteorological and Water Resources Foundation (Accessed on March 01, 2018). //www.funceme.br/app/calendario/produto/regioes/media/diario/. .
Imen, S., Chang, N.B., Yang, Y.J., 2015. Developing the remote sensing-based early warning system for monitoring TSS concentrations in Lake Mead. J. Environ. Manage. 160, 73–89. https://doi.org/10.1016/j.jenvman.2015.06.003.
Islam, M.R., Yamaguchi, Y., Ogawa, K., 2001. Suspended sediment in the Ganges and Brahmaputra Rivers in Bangladesh: observation from TM and AVHRR data. Hydrol. Process. 15 (3), 493–509. https://doi.org/10.1002/hyp.165.
Levenberg, K., 1944. A method for the solution of certain problems in least squares. Q. Appl. Math. 2, 164–168. https://doi.org/10.1090/qam/10666.
Lima Neto, I.E., Wiegand, M.C., de Araújo, J.C., 2011. Sediment redistribution due to a dense reservoir network in a large semi-arid Brazilian basin. Hydrological Sciences Journal des Sciences Hydrologiques 56 (2), 319–333. https://doi.org/10.1080/02626667.2011.553616.
Liu, C., He, Y., Des Walling, E., Wang, J.J., 2013. Changes in the sediment load of the Lancang-Mekong River over the period 1965–2003. Sci. China Technol. Sci. 56 (4), 843–852. https://doi.org/10.1007/s11431-013-5162-0.
Lodhi, M.A., Rundquist, D.C., Han, L., Kuzila, M.S., 1998. Estimation of suspended sediment concentration in water using integrated surface reflectance. Geocarto Int. 13 (2), 11–15. https://doi.org/10.1080/10106049809354637.
Long, C.M., Pavelsky, T.M., 2013. Remote sensing of suspended sediment concentration and hydrologic connectivity in a complex wetland environment. Remote Sens. Environ. 129, 197–209. https://doi.org/10.1016/j.rse.2012.10.019.
Mano, V., Némery, J., Belleudy, P., Poirel, A., 2009. Assessment of suspended sediment transport in four alpine watersheds (France): influence of the climatic regime. Hydrol. Process. 23, 777–792. https://doi.org/10.1002/hyp.7178.
Marquardt, D., 1963. An algorithm for least squares estimation of nonlinear parameters. J. Soc. Ind. Appl. Math. 11 (2), 431–441. https://doi.org/10.1137/0111030.
Martinez, J.M., Maurice-Bourgoin, L., Moreira-Turcq, P., Guyot, J.L., 2004. Use of MODIS and MERIS data for the water quality monitoring of Amazonian rivers and floodplain lakes. Paper Presented at the LBA Third International Conference.
Martinez, J.M., Guyot, J.L., Filizola, N., Sondag, F., 2009. Increase in suspended sediment discharge of the Amazon River assessed by monitoring network and satellite data. Catena 79 (3), 257–264. https://doi.org/10.1016/j.catena.2009.05.011.
Mas, J.F., Flores, J.J., 2008. The application of artificial neural networks to the analysis of remotely sensed data. Int. J. Remote Sens. 29 (3), 618–663. https://doi.org/10.1080/01431160701352154.
Medeiros, P.H.A., de Araújo, J.C., Mamede, G.L., Creutzfeldt, B., Güntner, A., Bronstert, A., 2014. Connectivity of sediment transport in a semiarid environment: a synthesis for the Upper Jaguaribe Basin, Brazil. J. Soils Sediments 14 (12), 1938–1948. https://doi.org/10.1007/s11368-014-0988-z.
Mertes, L.A., Smith, M.O., Adams, J.B., 1993. Estimating suspended sediment concentrations in surface waters of the Amazon River wetlands from Landsat images. Remote Sens. Environ. 43 (3), 281–301. https://doi.org/10.1016/0034-4257(93)90071-5.
Ody, A., Doxaran, D., Vanhellemont, Q., Nechad, B., Novoa, S., Many, G., Bourrin, F., Verney, R., Pairaud, I., Gentili, B., 2016. Potential of high spatial and temporal ocean color satellite data to study the dynamics of suspended particles in a micro-tidal river plume. Remote Sens. (Basel) 8 (3), 245. https://doi.org/10.3390/rs8030245.
Ouillon, S., Douillet, P., Andréfouët, S., 2004. Coupling satellite data with in situ measurements and numerical modeling to study fine suspended-sediment transport: a study for the lagoon of New Caledonia. Coral Reefs 23 (1), 109–122. https://doi.org/10.1007/s00338-003-0352-z.
Peter, S., de Araújo, J.C., Araújo, N.A.M., Herrmann, H.J., 2014. Flood avalanches in a semiarid basin with a dense reservoir network. J. Hydrol. 512, 408–420. https://doi.org/10.1016/j.jhydrol.2014.03.001.
Peterson, K.T., Sagan, V., Sidike, P., Cox, A.L., Martinez, M., 2018. Suspended sediment concentration estimation from Landsat imagery along the Lower Missouri and Middle Mississippi rivers using an extreme learning machine. Remote Sens. 10 (10), 1503. https://doi.org/10.3390/rs10101503.
Pinheiro, E.A.R., Metselaar, K., de Jong van Lier, Q., Araújo, J.C., 2016. Importance of soil-water to the Caatinga biome, Brazil. Ecohydrology 9 (7), 1313–1327. https://doi.org/10.1002/eco.1728.
RapidEye, 2015. RapidEye—Satellite Imagery Product Specifications Version 6.1, April. Available online: http://www.e -geos.it/images/Satellite_data/rapideye/re_Product_Specifications_ENG.pdf (Accessed on 18 May 2017).
Ritchie, J.C., Cooper, C.M., 1991. An algorithm for estimating surface suspended sediment concentrations with Landsat MSS digital data. J. Am. Water Resour. Assoc. 27 (3), 373–379. https://doi.org/10.1111/j.1752-1688.1991.tb01436.x.
Ritchie, J.C., Zimba, P.V., Everitt, J.H., 2003. Remote sensing techniques to assess water quality. Photogramm. Eng. Remote Sens. 69 (6), 695–704. https://doi.org/10.14358/PERS.69.6.695.
Santos, J.C.N., Andrade, E.M., Medeiros, P.H.A., Guerreiro, M.J.S., Palácio, H.A.Q., 2017. Effect of rainfall characteristics on runoff and water erosion for different land uses in a tropical semiarid region. Water Resour. Manag. 31, 173–185. https://doi.org/10.1007/s11269-016-1517-1.
Sari, V., Castro, N.M.R., Pedrollo, O.C., 2017. Estimate of suspended sediment concentration from monitored data of turbidity and water level using artificial neural networks. Water Resour. Manag. 31 (15), 4909–4923. https://doi.org/10.1007/s11269-017-1785-4.
Silva, W.P., Silva, C.M.D.P.S., Cavalcanti, C.G.B., Silva, D.D.P.S., Soares, I.B., Oliveira, J.P.S., Silva, C.D.P.S., 2004. LAB Fit curve adjustment: a software in Portuguese for treatment of experimental data. [In Portuguese.]. Revista Brasileira de Ensino de Física 26, 4. https://doi.org/10.1590/S0102-47442004000400018.
Syvitski, J.P., Morehead, M.D., Bahr, D.B., Mulder, T., 2000. Estimating fluvial sediment transport: the rating parameters. Water Resour. Res. 36 (9), 2747–2760. https://doi.org/10.1029/2000WR900133.
Topliss, B.J., Almos, C.L., Hill, P.R., 1990. Algorithms for remote sensing of high concentration, inorganic suspended sediment. Int. J. Remote Sens. 11 (6), 947–966. https://doi.org/10.1080/01431169008955069.
Vermote, E.F., Tanre, D., Deuze, J.L., Herman, M., Morcrette, J.J., 1997. Second simulation of the satellite signal in the solar Spectrum, 6s: an overview. IEEE Trans. Geosci. Remote. Sens. 35 (3), 675–686. https://doi.org/10.1109/36.581987.
Villar, R.E., Martinez, J.M., Guyot, J.L., Fraizy, P., Armijos, E., Crave, A., Bazán, H., Vauchel, P., Lavado, W., 2012. The integration of field measurements and satellite observations to determine river solid loads in poorly monitored basins. J. Hydrol. 444, 221–228. https://doi.org/10.1016/j.jhydrol.2012.04.024.
Wackerman, C., Hayden, A., Jonik, J., 2017. Deriving spatial and temporal context for point measurements of suspended sediment concentration using remote-sensing imagery in the Mekong Delta. Cont. Shelf Res. 147, 231–245. https://doi.org/10.1016/j.csr.2017.08.007.
Wang, F., Zhou, B., Xu, J., Song, L., Wang, X., 2009a. Application of neural network and MODIS 250 m imagery for estimating suspended sediments concentration in Hangzhou Bay, China. Environ. Geol. 56 (6), 1093–1101. https://doi.org/10.1007/s00254-008-1209-0.
Wang, J.J., Lu, X.X., Liew, S.C., Zhou, Y., 2009b. Retrieval of suspended sediment concentrations in large turbid rivers using Landsat ETM+: an example from the Yangtze River, China. Earth Surf. Process. Landf. 34 (8), 1082–1092. https://doi.org/10.1002/esp.1795.
Wang, J.J., Lu, X.X., Liew, S.C., Zhou, Y., 2010. Remote sensing of suspended sediment concentrations of large rivers using multi-temporal MODIS images: an example in the Middle and Lower Yangtze River, China. Int. J. Remote Sens. 31 (4), 1103–1111. https://doi.org/10.1080/01431160903330339.
Wass, P.D., Marks, S.D., Finch, J.W., Leeks, G.J.X.L., Ingram, J.K., 1997. Monitoring and preliminary interpretation of in-river turbidity and remote sensed imagery for suspended sediment transport studies in the Humber catchment. Sci. Total Environ. 194, 263–283. https://doi.org/10.1016/S0048-9697(96)05370-3.
Zhang, S., Foerster, S., Medeiros, P., de Araújo, J.C., Waske, B., 2018. Effective water surface mapping in macrophyte-covered reservoirs in NE Brazil based on Terra SAR-X time series. Int. J. Appl. Earth Obs. Geoinf. 69, 41–55. https://doi.org/10.1016/j.jag.2018.02.014.
Zhou, W., Wang, S., Zhou, Y., Troy, A., 2006. Mapping the concentrations of total suspended matter in Lake Taihu, China, using Landsat-5 TM data. Int. J. Remote Sens. 27 (6), 1177–1191. https://doi.org/10.1080/01431160500353825.